Remote Sensing of Environment 138 (2013) 126–133

Contents lists available at SciVerse ScienceDirect

Remote Sensing of Environment

journal homepage: www.elsevier.com/locate/rse

Retrieving vegetation clumping index from Multi-angle Imaging SpectroRadiometer (MISR) data at 275 m resolution

Jan Pisek [a,*], Youngryel Ryu [b], Michael Sprintsin [c], Liming He [d], Andrew J. Oliphant [e], Lauri Korhonen [f], Joel Kuusk [a], Andres Kuusk [a], Rafael Bergstrom [g], Jochem Verrelst [h], Krista Alikas [a]

[a] Tartu Observatory, 61602 Tõravere, Tartumaa, Estonia
[b] Department of Landscape Architecture and Rural Systems Engineering, Seoul National University, Seoul, Republic of Korea
[c] Forest Management and GIS Department, Jewish National Fund-Keren Kayemet LeIsrael, Eshtaol, M.P. Shimshon 99775, Israel
[d] Department of Geography and Program in Planning, University of Toronto, 100 St. George St., Room 5047, Toronto, ON M5S 3G3, Canada
[e] Department of Geography and Environment, San Francisco State University, San Francisco, CA 94132, USA
[f] University of Eastern Finland, School of Forest Sciences, P.O. Box 111, FI-80101 Joensuu, Finland
[g] Natural Resources and Environmental Management, University of Hawaii at Manoa, Honolulu, HI, USA
[h] Laboratory of Earth Observation, Image Processing Laboratory, Valencia University, Valencia, Spain

ARTICLE INFO

Article history:
Received 25 April 2013
Received in revised form 17 July 2013
Accepted 19 July 2013
Available online xxxx

Keywords:
Multi-angle remote sensing
MISR
Vegetation clumping index
Hotspot
NDHD

ABSTRACT

Clumping index, the measure of foliage grouping relative to a random distribution of leaves in space, is a key structural parameter of plant canopies that influences canopy radiation regimes and controls canopy photosynthesis and other land–atmosphere interactions. In this study, we retrieve the clumping index using the original 275 m resolution data of the Multi-angle Imaging SpectroRadiometer (MISR) instrument over a set of sites representing diverse biomes and different canopy structures. Also for the first time, the MISR derived clumping index values are directly validated with both in-situ vertical profiles and seasonal trajectories of clumping index. Our results illustrate that MISR data with 275 m allow clumping index estimates at much more pertinent scales (both spatial and temporal) than previous maps from Polarization and Directionality of Earth Reflectances (POLDER) and Moderate Resolution Imaging Spectroradiometer (MODIS) for modeling local carbon and energy fluxes.

1. Introduction

Leaves in canopies are generally grouped into various sub-canopy structures such as tree crowns, branches and shoots. These structures make the leaf spatial distribution non-random. The foliage clumping index (CI) is used to quantify the degree of deviation of this distribution from the random case (Chen & Black, 1992; Nilson, 1971). The CI value larger than unity implies that the foliage is regularly distributed; CI equals to one for a random distribution and in the case of foliage more clumped than random, CI < 1 (Chen, Menges, & Leblanc, 2005; see e.g. Chen, 1996 for in-depth discussion). Being an important parameter for correct assessment of true leaf area index (LAI_t), the CI is also required for the estimation of sunlit and shaded leaf fractions in the canopy and for accurate modeling of the canopy-level gross primary production (GPP) (Baldocchi & Harley, 1995; Chen et al., 2012; Ryu et al., 2011). Chen et al. (2012) recently showed that global GPP is overestimated by 12% even when accurate LAI_t is available but clumping is ignored.

As the CI can vary considerably for a land cover type, it is highly desirable to map the spatial distribution of this index using remote sensing data (Chen, Liu, Leblanc, Lacaze, & Roujean, 2003). Recently, both global and regional CI maps were developed using multi-angle remote sensing data from the Polarization and Directionality of Earth Reflectances (POLDER) instrument at ~6 km resolution (Chen et al., 2005; Leblanc, Chen, White, et al., 2005; Pisek, Chen, Lacaze, Sonnentag, & Alikas, 2010; Roujean & Lacaze, 2002) and from the Moderate Resolution Imaging Spectroradiometer (MODIS) at 500 m resolution (He, Chen, Pisek, Schaaf, & Strahler, 2012; Hill, Averill, Jiao, Schaaf, & Armston, 2008; Hill et al., 2011; Zhu et al., 2012).

Clumping has also been traditionally assumed to remain constant over seasons (Baldocchi et al., 2002; Sampson, Janssens, & Ceulemans, 2006) for modeling purposes due to limited data availability. The POLDER/MODIS derived CI maps generally reported and validated only annual CI values that were obtained by extracting either the minimum (representing the maximum level of clumping observed in the time period — e.g. Chen et al., 2005; Hill et al., 2011) or median CI (for noise removal purpose — e.g. He et al., 2012). Evidence from long-term time series in recent literature (Ryu, Nilson, et al., 2010; Ryu et al., 2012; Sprintsin et al., 2011) indicates that actually CI could have very strong annual and seasonal oscillations driven by site/species phenology. No direct validation of seasonal CI profiles from satellite data has been done yet.

* Corresponding author. Tel.: +372 7410 265.
E-mail address: janpisek@gmail.com (J. Pisek).

0034-4257/$ – see front matter © 2013 Elsevier Inc. All rights reserved.
http://dx.doi.org/10.1016/j.rse.2013.07.014

The objective of this study is to examine whether the technical specification (e.g. spatial resolution and angular sampling) of the Multi-angle Imaging SpectroRadiometer (MISR) can allow retrieval of CI estimates at more pertinent scales (both spatial and temporal) than previous CI maps from POLDER and MODIS. Those estimates could be used for advanced modeling of radiation interaction with vegetation and energy and mass (water and carbon) exchanges between the surface and the atmosphere (see e.g. Houborg, Anderson, Norman, Wilson, & Meyers, 2009).

To achieve this goal, we report on derivation of clumping index at higher resolution (275 m) using the multi-angular observations from MISR. The results are directly validated using in-situ measurements of CI at different heights in the canopy using towers at six sites representing diverse biomes. We also compare MISR-based CI estimates with observed seasonal trajectories of CI at three additional sites: an arid monocultured pine plantation in Israel, an oak-grass savanna woodland in California, USA, and a hemiboreal evergreen coniferous forest in Estonia.

2. Materials and methods

2.1. MISR data

MISR consists of nine cameras arranged to view along track that acquire image data with nominal view zenith angles relative to the surface reference ellipsoid of 0.0°, ±26.1°, ±45.6°, ±60.0°, and ±70.5° (forward and aftward of the Terra satellite) in four spectral bands (446, 558, 672, and 866 nm). In the global mode, the 672 nm (red) band images are acquired with a nominal maximum cross-track ground spatial resolution of 275 m in all nine cameras and information from all bands is provided at this resolution in the nadir camera as well (Diner, Beckert, Bothwell, & Rodriguez, 2002; Diner et al., 1998).

The MI1B2T product is the terrain-projected top-of-atmosphere (TOA) spectral radiance with a nominal 275 m spatial resolution in the nadir multispectral bands and off-nadir red band (Diner et al., 1999). We converted TOA radiances into TOA surface bidirectional reflectance factors (BRFs) using the exo-atmospheric irradiances, Earth–Sun distance and solar zenith angle accompanying the data. Additional MISR products were also used: MISR Level 2 MIL2ASLS Land Surface Parameters, MISR Level 1B2 MI1B2GEOP Geometric Parameters, and MISR Ancillary Geographic Product. The Land Surface product provides surface bihemispherical and directional–hemispherical reflectance (Albedo), hemispherical directional and bidirectional reflectance factor (BRF), BRF model parameters, LAI, fraction of photosynthetically active radiation, and normalized difference vegetation index on a 1.1 km grid. The MI1B2GEOP product includes grids of solar azimuth, solar zenith, and nine viewing azimuth and zenith angles at 17.6 km resolution. The MISR Ancillary Geographic Product provides longitude, latitude, elevation data, surface azimuths, and a land/water mask, on 1.1 km and 17.6 km resolution grids. We retrieved surface BRF information from the Land Surface Product, sun/view, zenith/azimuth angles from the MI1B2GEOP product, and longitude and latitude of pixels from the MISR Ancillary Geographic Product. MISR Level 2 products are already screened for contamination from sources such as clouds, cloud shadows, sun glitter over water, and topographically shadowed regions (Bothwell, Hansen, Vargo, & Miller, 2002).

2.2. MODIS data

The MODIS BRDF Model Parameters product (MCD43A1) data from October 2005 to December 2006 were downloaded from the Data Pool of Land Processes Distributed Active Archive Center (LP DAAC). Subsets of MODIS data covering the homogeneous forest sites in North America identified in the POLDER-3 BRDF data set (Bréon, Fédèle, Maignan, & Lacaze, 2007) and with available MISR observations acquired about the same time were selected. The MODIS BRDF/Albedo Product (MCD43A1, version 5) (Lucht, Schaaf, & Strahler, 2000; Schaaf et al., 2002) is a standard product that provides the weighting parameters associated with the RossThick-LiSparse-Reciprocal (RTLSR) BRDF model that describes the reflectance anisotropy at 500 m resolution (Wanner, Li, & Strahler, 1995). The BRDF parameters are produced every eight days with 16 days of acquisition using both Terra and Aqua data (Schaaf et al., 2002). The hotspot reflectance for red band (MODIS band 1; 620–670 nm) was produced with the RTLSR model driven by the MCD43A1 BRDF parameters (isotropic, volumetric, and geometric kernel weights (Wanner et al., 1995)). Corresponding solar zenith, view zenith, and relative azimuth angles to reproduce the MODIS hotspot were extracted from the POLDER-3 BRDF data set (Bréon et al., 2007). The identical angular configuration of the data allows us to correct the hotspot magnitude reconstructed from the MODIS BRDF product (He et al., 2012), and subsequently apply the identical hotspot-reconstruction relationships to the MISR BRF values as well (see Section 2.3).

The associated MODIS data quality (MCD43A2) product was also downloaded from the same source and was used to select the best quality (QA = 0) retrievals only.

2.3. Retrieval method

The flowchart in Fig. 1 shows an overview of the steps to derive foliage clumping information from MISR red band at 275 m

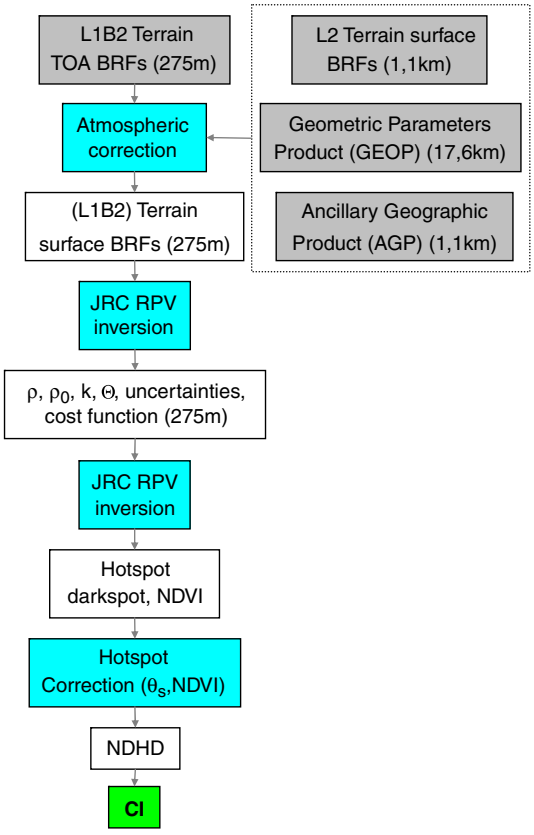

Fig. 1. Scheme of clumping index retrieval from MISR data. The gray boxes represent inputs from standard MISR global mode products; the white boxes represent the new high spatial resolution (275 m) products generated in this study; the cyan boxes indicate computational models or codes; and the final green box indicates the result (clumping index). (For interpretation of the references to color in this figure legend, the reader is referred to the web version of this article.)

resolution. The normalized difference between the hotspot and darkspot (NDHD) index has been shown to be linearly related to CI (Chen et al., 2003):

$$NDHD = (HS - DS)/(HS + DS) \quad (1)$$

and

$$CI = A(\theta_S) \cdot NDHD + B(\theta_S) \quad (2)$$

where A and B are the coefficients determined by the linear regression and tabulated for different θ_S, crown shapes, and bands by model simulations (Chen et al., 2005). In the algorithm development, clumping was determined from the LAI_t input and the resulting gap fraction simulated by the geometrical optical model 4-Scale (Chen & Leblanc, 1997). Therefore, the algorithm should allow the correct retrieval of the stand average clumping of the leaves.

As the first step, TOA BRFs from the MI1B2T product at 275 m need to be converted into surface BRF values. Following the approach described by Chopping, Nolin, Moisen, Martonchik, and Bull (2009) and Verstraete et al. (2012), we exploit the fact that the 1.1 km data are routinely screened and corrected as part of the Level 2 Land Surface product (MIL2ASLS). TOA BRFs from the MI1B2T product are therefore upscaled to 1.1 km resolution. The relationship is then found between the corresponding upscaled TOA BRF from the MI1B2T product and the surface BRF values from the Level 2 Land Surface product (MIL2ASLS). The identified coefficients are used to convert the full spatial resolution (275 m) TOA BRFs into full spatial resolution surface BRFs.

Second, the Rahman–Pinty–Verstraete (RPV) model (Rahman, Pinty, & Verstraete, 1993) is inverted against these full-resolution BRF values in the red band using the RPV inversion-3 software package (Lavergne et al., 2007). The RPV model splits the scattered radiation field for a given wavelength into a scalar amplitude component ρ_0 and an associated directional component describing the anisotropy of the surface (Pinty, Widlowski, Gobron, Verstraete, & Diner, 2002). The directional component of the reflectance function is expressed as the product of three functions: 1) the modified Minnaert function k that controls the curvature (e.g., the degree of convexity or concavity), 2) a parameter Θ that controls the degree of forward and backward scattering regimes; and 3) an optional hotspot descriptor function ρ_c. The underlying algorithms for each of the parameters are documented in Lavergne et al. (2007). The 4-parameter (including hotspot) version of the inverse model was implemented.

The initial hotspot (HS) and darkspot (DS) values in the principal plane are reconstructed for solar zenith angle of 60° using the four kernel coefficients for a pixel from the RPV model inversion. Hotspot is obtained as the surface BRF for coincident solar and viewing zenith angles (60°); darkspot corresponds to the minimum surface BRF in the forward scattering direction when the solar zenith angle is 60°. The view/solar zenith angle of 60° was chosen to minimize the effect of leaf angle orientation on the CI estimation (see Pisek, Lang, Nilson, Korhonen, & Karu, 2011; Pisek, Sonnentag, Richardson, & Mõttus, 2013).

Next, the MISR-hotspot might still be underestimated. Originally using MODIS BRDF product (Schaaf et al., 2002) and near-coincident directional information from POLDER-3 observations over homogeneous areas with vegetation (Bréon et al., 2007), He et al. (2012) developed a method to correct possible hotspot underestimation (ΔR_{HS}) based on the solar zenith angle (θ_S) and nadir normalized difference vegetation index (NDVI) value. For the red band:

$$\Delta R_{HS} = -0.031 \cdot \exp(1.4142 \cdot \theta_S - NDVI) + 0.002 \quad (3)$$

After verifying that MISR underestimates the hotspot in a similar fashion to the MODIS BRDF product (see Section 3.1), we apply the same correction for MISR data as well. Finally, reflectance differences among MISR, POLDER and MODIS simulated at the same angular configurations over vegetation are rather small in the red band (Jin et al., 2002; Lallart, Kahn, & Tanré, 2008; Lyapustin et al., 2007) and the same relationships between CI and NDHD from Chen et al. (2005) are applied to MISR data.

2.4. Study sites and data for validation

The study sites comprise diverse sets of nine stands representing different biomes (vertical profiles at six sites and seasonal trajectories at three sites). Detailed site descriptions are provided in Table 1. The motivation for collecting the vertical profiles partially came from He et al. (2012) who hypothesized that field measurements near the ground surface may considerably underestimate the overall canopy-level clumping effect (i.e. producing too large CI values) due to the presence of an understory at forest sites.

First, we report on our in-situ measurements of CI at different heights using towers at six of these stands. There are two northern boreal evergreen needleleaf stands in Hyytiälä (HYY; 61.85° N, 24.29° E) and Sodankylä (SOD; 67.36° N, 26.64° E), Finland. Scots pine (*Pinus sylvestris* L.) is dominant in both stands. Both sites lack a tall understory vegetation. The forest floor vegetation is dominated by lingonberry, blueberry, lichens and mosses at HYY (Ilvesniemi et al., 2009) and by fork moss with lichens at SOD (Manninen et al., 2012).

Two native cloud rainforest stands are located in Thurston Lava Tube (HVT; 19.41° N, 155.23° W) and Laupahoehoe (LEF; 19.93° N, 155.29° W), Hawai'i, USA. HVT consists primarily of a single canopy species,

Table 1
Site characteristics.

Site	Location	Forest type	Overstory	Mean tree height (m)	Understory	Reference	In-situ data collection
HYY	61.85° N, 24.29° E	NEF	SP	16	Lingonberry, blueberry and mosses (forest floor)	Ilvesniemi et al. (2009)	2001/11
SOD	67.36° N, 26.64° E	NEF	SP	12	Lichen, fork moss (forest floor)	Rautiainen et al. (2007)	2007/9
LEF	19.93° N, 155.29° W	EBF	M, K	19	Cibotium spp.	Kellner and Asner (2009)	2013/1
HVT	19.41° N, 155.23° W	EBF	M	14.5 ± 1.4	*Cibotium glaucum* (3.8 ± 2.7 m)	Giambelluca et al. (2009)	2010/9
MMSF	39.32° N, 86.41° W	BDF	SM, TP, S, WO, BO	27	Max. understory height 10 m	Oliphant et al. (2004)	2005/6
JARV	58.27° N, 27.27° E	MF	SB, BA, NS	17	Suppressed tree layer (mean height of 6.4 ± 0.6 m)	Noe et al. (2011)	2011/7
Yatir	31.35° N, 35.03° E	NEF	AP	8	Sparse grass (Nov–Apr)	Sprintsin et al. (2011)	2005
Tonzi	38.43° N, 120.96° W	S	BlO, GP	9.4 ± 4.3	Grass	Baldocchi et al. (2004)	2009/7–2010/3
RAMI pine	58.31° N, 27.30° E	NEF	SP	16	*Ledum palustre*, *Eriophorum vaginatum*, continuous *Sphagnum* ssp. moss layer (forest floor)	Kuusk et al. (2012)	2011/4–10

In the column "Forest type" NEF — needleleaf evergreen forest, EBF — evergreen broadleaf forest, BDF — broadleaf deciduous forest, MF — mixed forest, S — savanna. In the column "Overstory" SP — Scots pine, M — *Metrosideros polymorpha*, K — Koa, SM — sugar maple, TP — tulip poplar, S — Sassafras, WO — white oak, BO — black oak, SB — silver birch, BA — black alder, NS — Norway spruce, AP — Aleppo pine, BlO — blue oak, GP — gray pine.

ohi'a lehua (*Metrosideros polymorpha*), with a dense understory layer of hapu'u ferns (*Cibotium* spp.) (Giambelluca et al., 2009). LEF has similarly comprised overstory with an additional dominant species, Koa (*Acacia koa*) (Kellner & Asner, 2009).

The successional broadleaf stand in Morgan–Monroe State Forest (MMSF; 39.32° N, 86.41° W) in Indiana, USA, is comprised predominantly of sugar maple (*Acer saccharum*), tulip poplar (*Liriodendron tulipifera*), sassafras (*Sassafras albidum*), white oak (*Quercus alba*), and black oak (*Quercus nigra*). Canopy vertical structure is fairly consistent around the tower with peaks in LAI_t occurring at the crown level at approximately 20–30 m and at the undergrowth level at approximately 0–10 m (Oliphant et al., 2004).

A scaffolding tower in Järvselja, Estonia (JARV, 58.27° N, 27.27 °E) was located in a hemiboreal-mixed stand with co-dominant species of silver birch (*Betula pendula* Roth.), black alder (*Alnus glutinosa* L.) and Norway spruce (*Picea abies* (L.) Karst.). A suppressed tree layer (mean height of 6.4 ± 0.6 m) is present around the tower and surrounding forest (Noe et al., 2011).

The vertical profiles of element clumping index (Ω_E) were obtained by climbing scaffolding/flux towers and taking leveled digital hemispherical photos (DHPs) along the climbed height. At each profile, usually several series of DHPs were acquired using a Nikon CoolPix 4500 digital camera with a Nikon FC-E8 fisheye lens (CoolPix 8800 + FC-E9 at SOD) under diffuse illumination conditions, following the protocol of Zhang, Chen, and Miller (2005). No leaves were present directly above the camera to obscure its field of view. The towers were masked from the photos before the analysis. The reference DHPs were obtained above the top of the tree canopy. Gap fraction profiles were extracted from the blue channel at view zenith angle 57° with the DHP software (v4.5; Canada Centre for Remote Sensing, Ottawa, Canada). Various methods exist to estimate Ω_E (see Gonsamo & Pellikka, 2009; Pisek et al., 2011). The method of Leblanc, Chen, Fernandes, Deering, and Conley (2005) was previously shown to get reliable clumping estimates in Järvselja RAdiation transfer Model Intercomparison (RAMI) stands (Pisek et al., 2011):

$$\Omega_{CLX}(\theta) = \frac{n \ln\left[\overline{P(\theta)}\right]}{\sum_{k=1}^{n} \ln[P_k(\theta)]/\Omega_{CC,k}(\theta)} \quad (4)$$

where $\Omega_{CLX}(\theta)$ is Ω_E determined using the method of Leblanc, Chen, Fernandes, et al. (2005), $\Omega_{CC,k}(\theta)$ is the Ω_E of segment k using the Chen and Cihlar (1995) method, $P_k(\theta)$ is the gap fraction of segment k, n is the total number of segments, $\overline{P(\theta)}$ is the mean gap fraction, and θ is the view zenith angle. Segment size was 15°. In the case of coniferous sites (HYY and SOD), we have to take into account the clumping of needles within a shoot (γ_E) as well (CI $=\Omega_E / \gamma_E$; for broadleaves $\gamma_E = 1$). Appropriate γ_E values for Scots pine in the case of HYY and SOD sites were selected for the corresponding time of the season, following the measurements of Oker-Blom and Smolander (1988).

The seasonal trajectories of CI were available for three additional sites. Yatir forest, Israel (31.35° N, 35.03° E), is a monocultured plantation which is dominated by Aleppo pine (*Pinus halepensis* Mill.). Sparse understory vegetation develops only during the rainy season (Nov–Mar) and disappears shortly thereafter (Grünzweig, Lin, Schwartz, & Yakir, 2003). Sprintsin et al. (2011) reported the seasonal trajectory of CI derived from stand structural parameters (Kucharik, Norman, & Gower, 1999). The same data set from Sprintsin et al. (2011) is included here for validation purposes.

An oak-savanna ecosystem in California, USA (Tonzi; 38.43° N; 120.96° W), is dominated by blue oak trees (*Quercus douglasii*) with occasional (<10%) gray pines (*Pinus sabiniana*) (Baldocchi, Xu, & Kiang, 2004). On thirteen days during 2009–2010, Ryu et al. (2012) collected zenith direction photos every 30 m along three 300 m long transects 30 m apart with Canon PowerShot A570IS digital camera. Ryu et al. (2012) estimated the foliage CI at ecosystem scale from the upward-pointing digital images for each measurement day using the method of Macfarlane et al. (2007).

The third validation site is a Scots pine (*P. sylvestris* L.) stand in Järvselja, Estonia (58.31° N 27.30° E). The site is very homogeneous with respect to its horizontal structure and gap fraction (Pisek et al., 2011); only six young birch trees exist within the regeneration layer, and no bushes. Forest understorey vegetation is composed of sparse labrador tea and cotton grass, and a continuous *Sphagnum* moss layer. The site is included in the RAdiation transfer Model Intercomparison (RAMI, http://ramibenchmark.jrc.ec.europa.eu/HTML/Home.php) exercise (Kuusk, Kuusk, & Lang, 2009; Kuusk, Lang, & Kuusk, 2012). Using the same approach as for the tower sites above, CI has been tracked throughout 2011 using a series of DHPs acquired with Nikon CoolPix 4500 digital camera, Nikon FC-E8 fisheye lens and γ_E measurements of Oker-Blom and Smolander (1988). In addition to field measurements, we also estimated CI using observed hotspot and darkspot values from airborne data over the RAMI pine stand. The BRF profile in the red band (660 nm) with very high angular resolution along the principal plane was measured in a flight campaign on 27 July 2011 (Fig. 2). The measurements were obtained with a special airborne spectrometer system UAVSpec3, designed and built at Tartu Observatory (Kuusk & Kuusk, 2010). Kuusk, Kuusk, and Lang (submitted for publication) provide full details on the instrument and the field campaign.

3. Results and discussion

3.1. Is the reconstructed hotspot BRF from MISR off-principal plane observations underestimated?

The RPV model has been shown to be quite powerful in representing a whole range of complex BRF fields (see e.g. Gobron & Lajas, 2002; Lucht, 1998; Privette, Eck, & Deering, 1997; Rahman et al., 1993; Roberts, 2001). At the same time, the inversion precision depends on the amount and angular distribution of the multiangular observations (Lavergne et al., 2007). It is necessary to check first if the RPV model with MISR data might not underestimate the hotspot close to the Sun's direction similarly to the MODIS RTLSR model (He et al., 2012). MISR samples BRFs along-track while MODIS samples BRFs across-track. The samplings along the principal plane are most useful for

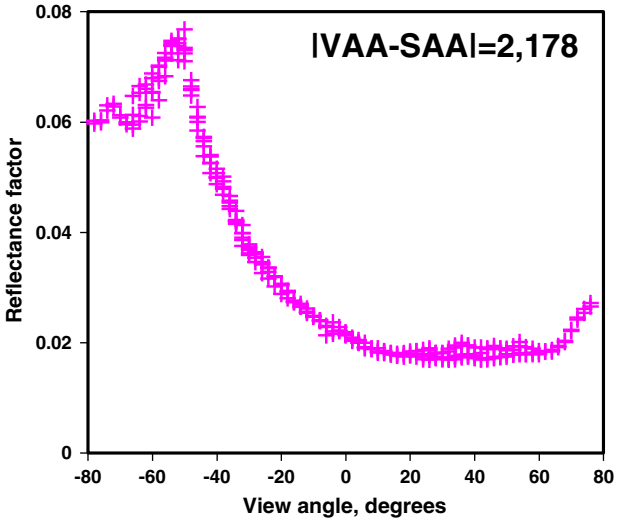

Fig. 2. Red BRF of the Järvselja RAMI stand in the solar principal plane from UAVSpec3 observations on July 27, 2011. All shown BRF observations were retrieved within 2° from the principal plane.

BRDF model retrieval. Both MISR and MODIS could be better than the other in terms of sampling the BRFs depending on the location and time (see e.g. Jin et al., 2002; Wanner et al., 1997). MISR has superiority in sampling the surface in nine directions quasi-simultaneously (in ≤7 min) while MODIS collects BRFs from 16 days (Schaaf et al., 2002).

There is a tight, close to 1:1, linear relationship ($R^2 = 0.92$) between hotspot values obtained from the MISR data with RPV model and MODIS RTLSR model over homogeneous forest sites included in POLDER BRDF database (Bréon et al., 2007) with available near-coincident observations from all three instruments in 2005–2006 in North America (Fig. 3). Very close agreement of the un-corrected hotspots from MISR RPV and MODIS TRLS models in Fig. 3 also confirms that the MISR hotspot magnitude can be corrected with the approach originally developed for MODIS by He et al. (2012) (Section. 2.3).

3.2. Variation of clumping index across canopy depths

First, it must be acknowledged that our measurements are limited to single point locations (tower) for a vertical profile at each site. Any factors that cause an increase in the variance of gap fraction (e.g. tree size, density and disturbances) would imply that a higher number of samples is needed (Nilson, Kuusk, Lang, Pisek, & Kodar, 2012; Ryu, Nilson, et al., 2010). At the same time, we note that the sites are spatially homogeneous at the compared size of MISR CI retrievals. We also note the retrievals are made using MISR BRF data acquired about the same time as the ground measurements.

The retrieved MISR CI values (0.55 at HYY; 0.56 at SOD) agree well with the CI measured at the ground (0.52 at HYY; 0.54 at SOD) at the coniferous sites in Finland (Fig. 4A–B). Level of clumping can be observed to be similar from 1 to ~9 m in height, because there is no understory tree/shrub layer at these two sites. There is a pronounced understory layer present at the other four sites with measured vertical profiles of clumping (Fig. 4C–F). The MISR CI values then differ from the CI measured at the ground. In the native cloud forests in Hawai'i, large gaps between tree crowns at upper levels of the canopy may not be measured near the ground due to occlusion by lower vegetation fern branches. This results in a small gap size near the ground and high (close to random distribution case) CI values (Fig. 4C–D). Instead, the MISR CI values are close to DHP estimates obtained above the nearly uniform understory fern layer at ~6 m (Fig. 4C–D). The vertical profile

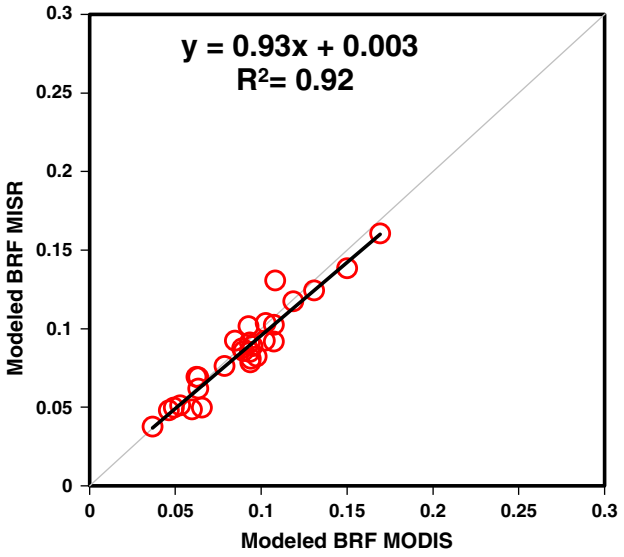

Fig. 3. A scatter plot between the uncorrected MODIS hotspot (BRF MODIS) and uncorrected MISR hotspot (BRF MISR) over homogeneous forest sites in North America with near-coincident MODIS, MISR, and POLDER-3 observations.

at HVT differs from LEF because there is an additional dominant species *A. koa* in the overstory at HVT.

A suppressed tree layer is also present at the two broadleaf stands in Indiana (MMSF) and Estonia (JARV). The best agreement between MISR and field measurements both at MMSF and in Järvselja is again achieved for observations taken above the understory layer (Fig. 4E–F). Out of all the reported sites here, the understory effect is the strongest at HVT (Fig. 4B), which agrees with the forest having indeed a pronounced 2-layered structure (Giambelluca et al., 2009).

Our results illustrate that field measurements near the ground level may considerably underestimate the canopy-level clumping effect (as retrieved from MISR data) because of the presence of the understory. The effects of understory need to be accounted for when the in-situ, ground measurements are used for validating CI products from remote sensing data. For future validations, this could be done by either obtaining the field measurements above the understory as done in this study, or comparing the retrievals with the vertical profiles predicted from validated models (see, e.g. Ni-Meister, Yang, & Kiang, 2010; Haverd et al., 2012).

3.3. Seasonal variation of clumping index

The seasonal dynamics of the CI derived from MISR observations over the Yatir forest in Israel were markedly different between two years compared in this study (2005 and 2012; Fig. 5A). In 2005, MISR retrievals captured the annual dynamics caused by needle phenology and concurrency of needle growth and litterfall during the dry period of the year (Apr–Aug) (Sprintsin et al., 2011). In 2012, Yatir had been intensively thinned due to massive drought-related mortality. This thinning increased the clumping at the landscape level and offset the decreasing clumping at the shoot level due to litterfall during the dry period of the year. The resulting seasonal trajectory of CI is then rather flat and in agreement with the MISR retrievals in 2012 (Fig. 5A). The only exception is the day-of-year (DOY) 143 for which MISR CI retrieval differed markedly from the overall flat trajectory present during the rest of the season. A sand storm entering the region around the local overpass time on that day (May 22, 2012) prevented the acquisition of good quality MISR observations and affected the retrieved CI value (0.45). The results over Yatir indicate that MISR observations have the capability to detect changes in the vegetation canopy structure.

Both in-situ transect measurements and MISR retrievals show the same pattern of seasonal clumping variation at the Tonzi blue oak site (Fig. 5B). With the canopy development, the CI decreased which indicates increased clumping as the crowns thickened (Ryu, Nilson, et al., 2010). Unfortunately there were no successful retrievals from MISR data due to the presence of clouds during the MISR overpasses in February–March and from mid-August till the end of October 2009 (Fig. 5B). Unlike Yatir, Tonzi has not experienced any significant change in stand structure during recent years. The seasonal trajectory of CI can be reconstructed using the MISR observations from 2011, when the atmospheric conditions were more favorable. The retrieved CI values are also within the range of other previously reported in-situ clumping estimates using different methods (Ryu, Sonnentag, et al., 2010). Importantly, the reconstructed seasonal trajectories of CI from MISR are rather smooth. This is an improvement on earlier attempts to reconstruct seasonal trajectories of clumping at the individual site level with POLDER and MODIS data (Chen et al., 2005; He et al., 2012).

The field data should be optimally compared with high resolution imagery from airborne sensors to allow a more direct validation of products from spaceborne sensors at multiple levels (Morisette et al., 2006). The very high angular resolution observations close to the principal plane from the airborne UAVSpec3 system (Fig. 2) allow CI determination over the RAMI pine stand. As in case of Yatir and Tonzi, there is no undergrowth/shrub layer at the site and the CI value (0.57) from UAVSpec3 matches well the in-situ DHP measurements from the same year (Fig. 5C).

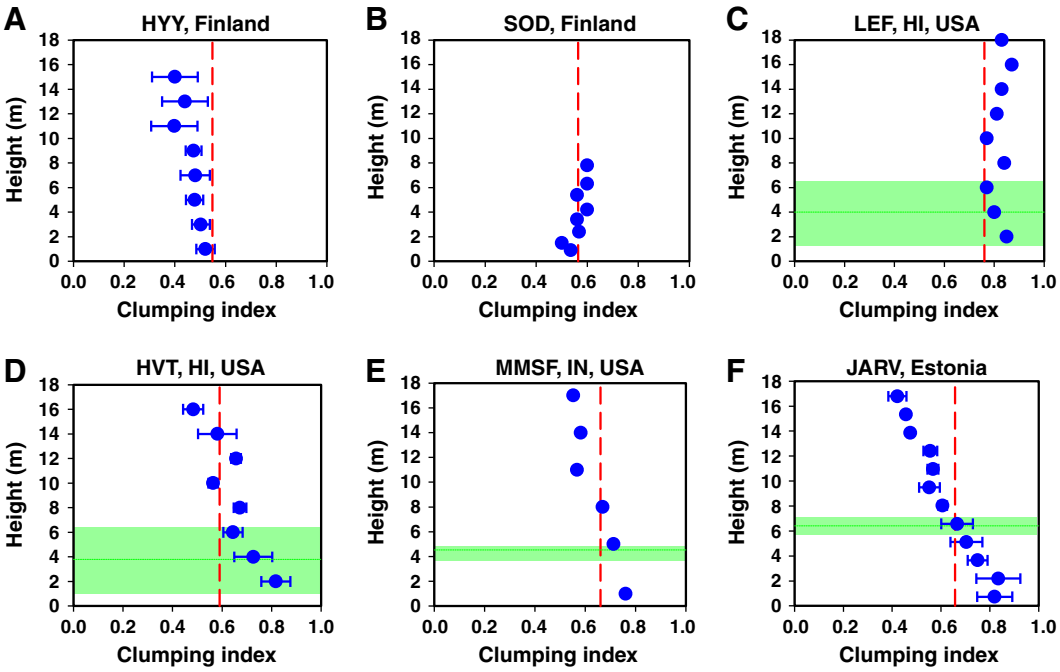

Fig. 4. Vertical profiles of foliage clumping from in-situ measurements with ±1 standard deviation bars. (A) Hyytiälä, Finland, (B) Sodankylä, Finland, (C) Laupahoehoe, HI, USA, (D) Thurston Lava Tube, HI, USA, (E) Morgan–Monroe State Forest, IN, USA, (F) Järvselja, Estonia. Clumping index values from MISR data obtained around the same time are marked with vertical dashed red line. The mean height of undergrowth layer is marked by a green horizontal dashed line; green areas mark the ±1 standard deviation area. (For interpretation of the references to color in this figure legend, the reader is referred to the web version of this article.)

There were only three cloud-free MISR observations over the RAMI pine site in 2011 (April 24, May 8, and June 11). Similar to Tonzi, the RAMI pine stand has not experienced any significant change in its structure during the recent years. The compiled successful MISR observations from 2005–2011 confirm the very stable structure of the RAMI pine stand. The respective MISR retrievals also agree with the closest DOY field measurements and by the airborne UAVSpec3 system (Fig. 5C). Additionally, all CI values (in situ, UAVSpec3 and MISR) in Fig. 5C are within the range of previously reported in-situ clumping estimates for the same RAMI pine stand (Pisek et al., 2011). The structural consistency as derived from data at multiple levels (in-situ, airborne, spaceborne) over multiple seasons and years is indeed a desired property of the real world stands included in the RAMI exercise (Widlowski et al., 2007).

The resulting smooth seasonal trajectories from in-situ measurements and satellite data further confirm the suitability of robust MISR observations at 275 m resolution from different years for reconstructing seasonal time series (Fig. 5B, C) or detecting the possible changes (e.g. thinning) in forest structure (Fig. 5A; Hill et al., 2011).

The reported CI values during the leaves-on period are very similar at the three sites (Fig. 5) despite representing different types of forest (needleleaf/broadleaf). It should be noted Tonzi (as the only deciduous site out of the three locations) is an open oak-savanna ecosystem with very low tree density (144 trees/ha; Ryu, Sonnentag, et al., 2010). This results in the presence of very large gaps between trees and low CI value (high clumping). The needleleaf tree stands (Yatir; RAMI pine) have higher tree density and higher CI value (lower clumping) at the beyond-shoot level. However, the needles are additionally clumped at the shoot-level. Although the forest structures are different at the three sites, the compounded effects of clumping at different levels lead to overall similar values as reported in Fig. 5. Unfortunately as of now we do not have available quality long-term series of field measurements from more sites, which would presumably result in greater observed variation of CI between different sites.

4. Conclusions

The primary mission of the MISR instrument is to study the Earth atmosphere and, in particular, to characterize atmospheric aerosols

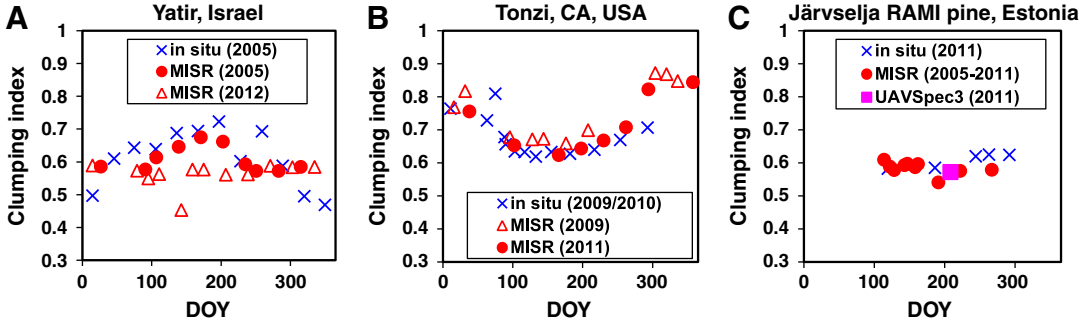

Fig. 5. Seasonal profiles of foliage clumping for (A) Yatir, Israel, (B) Tonzi, CA, USA, and (C) Järvselja RAMI pine stand, Estonia. Field measurements at all three sites were taken above understory (if present).

and clouds (Diner et al., 1998; Verstraete et al., 2012). Thus significant efforts have been invested to address these issues in great detail (Diner et al., 2005) and provide quality Level 2 products that were utilized to convert TOA BRF into surface BRF values at 275 m resolution in this study. The results presented here indicate that MISR observations could also be useful for vegetation studies allowing the derivation of an improved CI product in accuracy as well as spatial and temporal resolution. This is the first time that the smooth seasonal trajectories of CI at the pixel level are reported and validated.

Our results further illustrate the importance of taking into account the effect of understory while validating CI products from remote sensing data with values measured in the field. Satellite measurements respond to the structural effects of tree crowns, while ground measurements may be biased by the lower vegetation layers. Given the heterogeneous nature of land cover in many areas of the world, production and use of higher resolution maps of CI are very desirable.

Acknowledgments

The MISR and MODIS data were obtained from the NASA Langley Atmospheric Science Data Center/the NASA EOS Data Gateway and Land Processes Distributed Active Archive Center (DAAC) hosted by USGS, respectively. Jan Pisek is supported by the funding from the FP7-Marie Curie Actions program, Estonian Science Foundation grant no. ERMOS32. Dr. Janne Levula kindly gave permission to access the scaffolding tower at Hyytiälä; Dr. Thomas Giambelluca kindly allowed the first author to access the Thurston Lava Tube flux tower in Hawai'i. Liming He was supported by the Canadian Space Agency grant (11SUSMAPTO). Andrew Oliphant was supported by the NSF grant: BCS-0928352. Access to the site in MMSF was granted by the Indiana Department of Natural Resources, Division of Forestry and the authors are grateful to all of Indiana University's MMSF flux tower site researchers and students. Joel Kuusk and Andres Kuusk have been supported by Estonian Science Foundation and targeted financing by the Ministry of Education and Research, Project SF0180009Bs11, by the project "BioAtmos" of the Environmental protection and technology research and development program No. 3.2.0802.11-0043, and project TAP13-2 "Complex of the etalons for remote sensing" of the subprogram "Modernization of the research apparatus and equipment" of the implementation plan of the European Union structural funds "Development of the economic environment". Lauri Korhonen was sponsored by the GSForest, the NorSEN project, and the UEF strategic funds. The Sodankylä tower data acquisition was arranged by Terhikki Manninen and Timo Sukuvaara. Data from the Tonzi Ranch was supported by the Office of Science (BER), US Department of Energy, Grants DE-FG02-06ER64308 and DE-SC0005130. The first author wishes to thank Tiit Nilson for stimulating discussions about the clumping index; Eben Broadbent provided additional information about Laupahoehoe forest. Michael Sprintsin is thankful to Prof. Dan Yakir and Dr. Eyal Rotenberg (Department of Environmental Sciences and Energy Research at Weizmann Institute of Science) for their support during ground measurements. We thank four anonymous reviewers for providing comments that helped with improving the quality of the original submission.

References

Baldocchi, D.D., & Harley, P. C. (1995). Scaling carbon dioxide and water vapour exchange from leaf to canopy in a deciduous forest. II. Model testing and application. *Plant, Cell & Environment*, *18*, 1157–1173.

Baldocchi, D. D., Wilson, K. B., & Gu, L. H. (2002). How the environment, canopy structure and canopy physiological functioning influence carbon, water and energy fluxes of a temperate broad-leaved deciduous forest - an assessment with the biophysical model CANOAK. *Tree Physiology*, *22*, 1065–1077.

Baldocchi, D.D., Xu, L. K., & Kiang, N. (2004). How plant functional-type, weather, seasonal drought, and soil physical properties alter water and energy fluxes of an oak-grass savanna and an annual grassland. *Agricultural and Forest Meteorology*, *123*(1–2), 13–39.

Bothwell, G. W., Hansen, E. G., Vargo, R. E., & Miller, K. C. (2002). The Multiangle Imaging SpectroRadiometer science data system, its products, tools and performance. *IEEE Transactions on Geoscience and Remote Sensing*, *40*, 1467–1476.

Bréon, F. M., Fédèle, E., Maignan, F., & Lacaze, R. (2007). A database of directional reflectance signature (GLC2000) with an analysis tool. *A-Train Symposium. Lille*.

Chen, J. M. (1996). Optically-based methods for measuring seasonal variation in leaf area index of boreal conifer forests. *Agricultural and Forest Meteorology*, *80*, 135–163.

Chen, J. M., & Black, T. A. (1992). Foliage area and architecture of plant canopies from sunfleck size distributions. *Agricultural and Forest Meteorology*, *60*, 249–266.

Chen, J. M., & Cihlar, J. (1995). Plant canopy gap-size analysis theory for improving optical measurements of leaf-area index. *Applied Optics*, *34*, 6211–6222.

Chen, J. M., & Leblanc, S. G. (1997). A four-scale bidirectional reflectance model based on canopy architecture. *IEEE Transactions on Geoscience and Remote Sensing*, *35*, 1316–1337.

Chen, J. M., Liu, J., Leblanc, S. G., Lacaze, R., & Roujean, J. L. (2003). Multi-angular optical remote sensing for assessing vegetation structure and carbon absorption. *Remote Sensing of Environment*, *84*, 516–525.

Chen, J. M., Menges, C. H., & Leblanc, S. G. (2005). Global mapping of foliage clumping index using multi-angular satellite data. *Remote Sensing of Environment*, *97*, 447–457.

Chen, J. M., Mo, G., Pisek, J., Deng, F., Ishozawa, M., & Chan, D. (2012). Foliage clumping index as an important structural parameter for estimating global terrestrial gross primary productivity. *Global Biogeochemical Cycles*, *26*, GB1019, http://dx.doi.org/10.1029/2010GB003996.

Chopping, M., Nolin, A., Moisen, G. G., Martonchik, J. V., & Bull, M. (2009). Forest canopy height from the Multiangle Imaging SpectroRadiometer (MISR) assessed with high resolution discrete return lidar. *Remote Sensing of Environment*, *113*, 2172–2185.

Diner, D. J., Asner, G. P., Davies, R., Knyazikhin, Y., Muller, J. P., Nolin, A. W., et al. (1999). New directions in Earth observing: Scientific applications of multi-angle remote sensing. *Bulletin of the American Meteorological Society*, *80*, 2209–2229.

Diner, D. J., Beckert, J. C., Bothwell, G. W., & Rodriguez, J. I. (2002). Performance of the MISR instrument during its first 20 months in Earth orbit. *IEEE Transactions on Geoscience and Remote Sensing*, *40*, 1449–1466.

Diner, D. J., Beckert, J. C., Reilly, T. H., Bruegge, C. J., Conel, J. E., Kahn, R. A., et al. (1998). Multiangle Imaging SpectroRadiometer (MISR) instrument description and experiment overview. *IEEE Transactions on Geoscience and Remote Sensing*, *36*, 1072–1087.

Diner, D. J., Braswell, B. H., Davies, R., Gobron, N., Hu, J., Jin, Y., et al. (2005). The value of multiangle measurements for retrieving structurallyand radiatively consistent properties of clouds, aerosols, and surfaces. *Remote Sensing of Environment*, *97*, 495–518.

Giambelluca, T. W., Martin, R. E., Asner, G. P., Huang, M., Mudd, R. G., Nullet, M.A., et al. (2009). Evapotranspiration and energy balance of native wet montane cloud forest in Hawaii. *Agricultural and Forest Meteorology*, *149*, 230–243.

Gobron, N., & Lajas, D. (2002). A new inversion scheme for the RPV model. *Canadian Journal of Remote Sensing*, *28*, 156–167.

Gonsamo, A., & Pellikka, P. (2009). The computation of foliage clumping index using hemispherical photography. *Agricultural and Forest Meteorology*, *149*, 1781–1787.

Grünzweig, J. M., Lin, T., Schwartz, A., & Yakir, D. (2003). Carbon sequestration in arid-land forest. *Global Change Biology*, *9*(5), 791–799.

Haverd, V., Lovell, J. L., Cuntz, M., Jupp, D. L. B., Newnham, G. J., & Sea, W. (2012). The Canopy Semi-analytic P gap And Radiative Transfer (CanSPART) model: Formulation and application. *Agricultural and Forest Meteorology*, *160*, 14–35.

He, L., Chen, J. M., Pisek, J., Schaaf, C. B., & Strahler, A. H. (2012). Global clumping index map derived from the MODIS BRDF product. *Remote Sensing of Environment*, *119*, 118–130.

Hill, M. J., Averill, C., Jiao, Z., Schaaf, C. B., & Armston, J. (2008). Relationship of MISR RPV parameters and MODIS directional reflectance indices to vegetation patterns in an Australian tropical savanna. *Canadian Journal of Remote Sensing*, *34*(Supplement 2), S247–S267.

Hill, M. J., Román, M.O., Schaaf, C. B., Hutley, L., Brannstrom, C., Etter, A., et al. (2011). Characterizing vegetation cover in global savannas with an annual foliage clumping index derived from the MODIS BRDF product. *Remote Sensing of Environment*, *115*, 2008–2024.

Houborg, R., Anderson, M. C., Norman, J. M., Wilson, T., & Meyers, T. (2009). Intercomparison of a 'bottom-up' and 'top-down' modeling paradigm for estimating carbon and energy fluxes over a variety of vegetative regimes across the U.S. *Agricultural and Forest Meteorology*, *149*, 1875–1895.

Ilvesniemi, H., Levula, J., Ojansuu, R., Kolari, P., Kulmala, L., Pumpanen, J., et al. (2009). Long-term measurements of the carbon balance of a boreal Scots pine dominated forest ecosystem. *Boreal Environmental Research*, *14*, 731–753.

Jin, Y., Schaaf, C., Gao, F., Li, X., Strahler, A., Bruegge, C., et al. (2002). Improving MODIS surface BRDF/Albedo retrieval with MISR multi-angle observations. *IEEE Transactions on Geoscience and Remote Sensing*, *40*, 1593–1604.

Kellner, J. R., & Asner, G. P. (2009). Convergent structural responses of tropical forests to diverse disturbance regimes. *Ecology Letters*, *12*, 887–897.

Kucharik, C. J., Norman, J. M., & Gower, S. T. (1999). Characterization of radiation regimes in nonrandom forest canopies: theory, measurements, and a simplified modeling approach. *Tree Physiology*, *19*, 695–706.

Kuusk, J., & Kuusk, A. (2010). Autonomous lightweight airborne spectrometers for ground reflectance measurements. *2nd Workshop on Hyperspectral Image and Signal Processing: Evolution in Remote Sensing (WHISPERS 2010), Reykjavik, Iceland, June 2010* (CD-ROM, 4 pp.).

Kuusk, A., Kuusk, J., & Lang, M. (2009). A dataset for the validation of reflectance models. *Remote Sensing of Environment*, *113*, 889–892.

Kuusk, A., Kuusk, J., & Lang, M. (submitted for publication). Measured spectral bidirectional reflection properties of three mature hemiboreal forests. *Agricultural and Forest Meteorology* (submitted for publication, revision under review).

Kuusk, A., Lang, M., & Kuusk, J. (2012). Database of optical and structural data for the validation of forest radiative transfer models. In A. A. Kokhanovsky (Ed.), *Radiative Transfer and Optical Properties of Atmosphere and Underlying Surface. Light scattering reviews*, *7*. (pp. 109–148). Berlin, Germany: Springer.

Lallart, P., Kahn, R., & Tanré, D. (2008). POLDER2/ADEOSII, MISR, and MODIS/Terra reflectance comparisons. *Journal of Geophysical Research D: Atmospheres*, *113*, D14S02.

Lavergne, T., Kaminski, T., Pinty, B., Taberner, M., Gobron, N., Verstraete, M. M., et al. (2007). Application to MISR land products of an RPV model inversion package using adjoint and Hessian codes. *Remote Sensing of Environment*, *107*, 362–375.

Leblanc, S. G., Chen, J. M., Fernandes, R., Deering, D. W., & Conley, A. (2005a). Methodology comparison for canopy structure parameters extraction from digital hemispherical photography in boreal forests. *Agricultural and Forest Meteorology*, *129*, 187–207.

Leblanc, S. G., Chen, J. M., White, H. P., Latifovic, R., Lacaze, R., & Roujean, J. L. (2005b). Canada-wide foliage clumping index mapping from multiangular POLDER measurements. *Canadian Journal of Remote Sensing*, *31*, 364–376.

Lucht, W. (1998). Expected retrieval accuracies of bidirectional reflectance and albedo from EOS-MODIS and MISR angular sampling. *Journal of Geophysical Research*, *103*, 8763–8778.

Lucht, W., Schaaf, C. B., & Strahler, A. H. (2000). An algorithm for the retrieval of albedo from space using semiempirical BRDF models. *IEEE Transactions on Geoscience and Remote Sensing*, *38*, 977–998.

Lyapustin, A., Wang, Y., Kahn, R., Xiong, J., Ignatov, A., Wolfe, R., et al. (2007). Analysis of MODIS–MISR calibration differences using surface Albedo around AERONET sites and cloud reflectance. *Remote Sensing of Environment*, *107*, 12–21.

Macfarlane, C., Hoffman, M., Eamus, D., Kerp, N., Higginson, S., McMurtrie, R., et al. (2007). Estimation of leaf area index in eucalypt forest using digital photography. *Agricultural and Forest Meteorology*, *143*, 176–188.

Manninen, T., Korhonen, L., Riihelä, A., Lahtinen, P., Stenberg, P., Roujean, J. -L., et al. (2012). Boreal forest Albedo and LAI in SNORTEX 2008–2010. *Proceedings of International Geoscience and Remote Sensing Symposium 2012 (IGARSS 2012)* (pp. 3335–3338).

Morisette, J. T., Baret, F., Privette, J. L., Myneni, R. B., Nickeson, J. E., Garrigues, S., et al. (2006). Validation of global moderate resolution LAI products: A framework proposed within the CEOS land product validation subgroup. *IEEE Transactions on Geoscience and Remote Sensing*, *44*, 1804–1817.

Nilson, T. (1971). A theoretical analysis of the frequency of gaps in plant stands. *Agricultural Meteorology*, *8*, 25–38.

Nilson, T., Kuusk, A., Lang, M., Pisek, J., & Kodar, A. (2012). Simulation of statistical characteristics of gap distribution in forest stands. *Agricultural and Forest Meteorology*, *151*, 895–905.

Ni-Meister, W., Yang, W., & Kiang, N. Y. (2010). A clumped-foliage canopy radiative transfer model for a global dynamic terrestrial ecosystem model I: Theory. *Agricultural and Forest Meteorology*, *150*, 881–894.

Noe, S. M., Kimmel, V., Hüve, K., Copolovici, L., Portillo-Estrada, M., Püttsepp, Ü., et al. (2011). Ecosystem-scale biosphere–atmosphere interactions of a hemiboreal mixed forest stand at Järvselja, Estonia. *Forest Ecology and Management*, *262*, 71–81.

Oker-Blom, P., & Smolander, H. (1988). The ratio of shoot silhouette area to total needle area in Scots pine. *Forest Science*, *34*, 894–906.

Oliphant, A. J., Grimmond, C. S. B., Zutter, H. N., Schmid, H. P., Su, H. B., Scott, S. L., et al. (2004). Heat storage and energy balance fluxes for a temperate deciduous forest. *Agricultural and Forest Meteorology*, *126*, 185–201.

Pinty, B., Widlowski, J. L., Gobron, N., Verstraete, M. M., & Diner, D. J. (2002). Uniqueness of multiangular measurements — Part 1: An indicator of subpixel surface heterogeneity from MISR. *IEEE Transactions on Geoscience and Remote Sensing*, *40*, 1560–1573.

Pisek, J., Chen, J. M., Lacaze, R., Sonnentag, O., & Alikas, K. (2010). Expanding global mapping of the foliage clumping index with multi-angular POLDER 3 measurements: Evaluation and topographic compensation. *ISPRS Journal of Photogrammetry and Remote Sensing*, *65*, 341–346.

Pisek, J., Lang, M., Nilson, T., Korhonen, L., & Karu, H. (2011). Comparison of methods for measuring gap size distribution and canopy nonrandomness at Järvselja RAMI (RAdiation transfer Model Intercomparison) test sites. *Agricultural and Forest Meteorology*, *151*, 365–377.

Pisek, J., Sonnentag, O., Richardson, A., & Mõttus, M. (2013). Is the spherical leaf inclination angle distribution a valid assumption for temperate and borel broadleaf tree species. *Agricultural and Forest Meteorology*, *169*, 186–194.

Privette, J. L., Eck, T. F., & Deering, D. W. (1997). Estimating spectral Albedo and nadir reflectance through inversion of simple BRDF models with AVHRR/MODIS-like data. *Journal of Geophysical Research*, *102*, 29529–29542.

Rahman, H., Pinty, B., & Verstraete, M. M. (1993). Coupled surface-atmosphere reflectance (CSAR) model. 2. Semiempirical surface model usable with NOAA Advanced Very High Resolution Radiometer data. *Journal of Geophysical Research*, *98*, 20791–20801.

Rautiainen, M., Suomalainen, J., Mõttus, M., Stenberg, P., Voipio, P., Peltoniemi, J., et al. (2007). Coupling forest canopy and understory reflectance in the Arctic latitudes of Finland. *Remote Sensing of Environment*, *110*, 332–343.

Roberts, G. (2001). A review of the application of BRDF models to infer land cover parameters at regional and global scales. *Progress in Physical Geography*, *25*, 483–511.

Roujean, J. L., & Lacaze, R. (2002). Global mapping of vegetation parameters from POLDER multiangular measurements for studies of surface–atmosphere interactions: A pragmatic method and its validation. *Journal of Geophysical Research*, *107*, http://dx.doi.org/10.1029/2001JD000751.

Ryu, Y., Baldocchi, D.D., Kobayashi, H., van Ingen, C., Li, J., Black, T. A., et al. (2011). Integration of MODIS land and atmosphere products with a coupled-process model to estimate gross primary productivity and evapotranspiration from 1 km to global scales. *Global Biogeochemical Cycles*, *25*, GB4017, http://dx.doi.org/10.1029/2011GB004053.

Ryu, Y., Nilson, T., Kobayashi, H., Sonnentag, O., Law, B. E., & Baldocchi, D.D. (2010a). On the correct estimation of effective leaf area index: Does it reveal information on clumping effects? *Agricultural and Forest Meteorology*, *150*, 463–472.

Ryu, Y., Sonnentag, O., Nilson, T., Vargas, R., Kobayashi, H., Wenk, R., et al. (2010b). How to quantify tree leaf area index in an open savanna ecosystem: A multi-instrument and multi-model approach. *Agricultural and Forest Meteorology*, *150*, 63–76.

Ryu, Y., Verfaillie, J., Macfarlane, C., Kobayashi, H., Sonnentag, O., Vargas, R., et al. (2012). Continuous observation of tree leaf area index at ecosystem scale using upward-pointing digital cameras. *Remote Sensing of Environment*, *126*, 116–125.

Sampson, D. A., Janssens, I. A., & Ceulemans, R. (2006). Under-story contributions to stand level GPP using the process model SECRETS. *Agricultural and Forest Meteorology*, *139*, 94–104.

Schaaf, C. B., Gao, F., Strahler, A. H., Lucht, W., Li, X., Tsang, T., et al. (2002). First operational BRDF Albedo, nadir reflectance products from MODIS. *Remote Sensing of Environment*, *83*, 135–148.

Sprintsin, M., Cohen, S., Maseyk, K., Rotenberg, E., Grunzweig, J., Karnieli, A., et al. (2011). Long term and seasonal courses of leaf area index in a semi-arid forest plantation. *Agricultural and Forest Meteorology*, *151*, 565–574.

Verstraete, M. M., Hunt, L. A., Scholes, R. J., Clerici, M., Pinty, B., & Nelson, D. L. (2012). Generating 275-m resolution land surface products from the Multi-angle Imaging SpectroRadiometer data. *IEEE Transactions on Geoscience and Remote Sensing*, *50*, 3980–3990.

Wanner, W., Li, X., & Strahler, A. H. (1995). On the derivation of kernels for kernel-driven models of bidirectional reflectance. *Journal of Geophysical Research*, *100*, 21077–21089.

Wanner, W., Strahler, A., Hu, B., Lewis, P., Muller, J. P., Li, X., et al. (1997). Global retrieval of bidirectional reflectance and Albedo over land from EOS MODIS and MISR Data: Theory and algorithms. *Journal of Geophysical Research*, *102*, 17143–17162.

Widlowski, J. L., Taberner, M., Pinty, B., Bruniquel-Pinel, V., Disney, M., Fernandes, R., et al. (2007). Third RAdiation transfer Model Intercomparison (RAMI) exercise: Documenting progress in canopy reflectance models. *Journal of Geophysical Research-Atmospheres*, *112*(D9), D09111.

Zhang, Y., Chen, J. M., & Miller, J. (2005). Determining exposure of digital hemispherical photographs for leaf area index estimation. *Agricultural and Forest Meteorology*, *133*, 166–181.

Zhu, G., Ju, W., Chen, J. M., Gong, P., Xing, B., & Zhu, J. (2012). Foliage clumping index over China's landmass retrieved from the MODIS BRDF parameters product. *IEEE Transactions on Geoscience and Remote Sensing*, *50*, 2122–2137.